Cancer Nanotechnology

RESEARCH Open Access

Bufalin-loaded vitamin E succinate-grafted chitosan oligosaccharide/RGD-conjugated TPGS mixed micelles inhibit intraperitoneal metastasis of ovarian cancer

Lan Xu[1,2†], Shuli Ma[3†], Bozhen Fan[2], Zeting Yuan[1*] and Peihao Yin[1,4,5*]

†Lan Xu and Shuli Ma have contributed equally to this work

*Correspondence: yuan340202@163.com; yinpeihao@shutcm.edu.cn

[1] Interventional Cancer Institute of Chinese Integrative Medicine, Putuo Hospital, Shanghai University of Traditional Chinese Medicine, Shanghai, China
[2] Department of Obstetrics and Gynecology, Putuo Hospital, Shanghai University of Traditional Chinese Medicine, Shanghai, China
[3] School of Pharmacy, East China University of Science and Technology, Shanghai, China
[4] Shanghai Putuo Central School of Clinical Medicine, Anhui Medicine University, Anhui, China
[5] Department of General Surgery, Putuo Hospital, Shanghai University of Traditional Chinese Medicine, Shanghai, China

Abstract

Background: Intraperitoneal metastasis is one of the major causes of the high mortality rate of ovarian cancer. Bufalin (BU) is an effective component of the traditional Chinese medicine Chansu that exerts antitumor effects, including metastasis inhibition. In our previous studies, we found that BU inhibited the migration and invasion of ovarian cancer cells. However, the application of BU is limited due to its insolubility, toxicity and imprecise targeting. The aim of this study was to use vitamin E succinate (VES)-grafted chitosan oligosaccharide (CSO)/arginine-glycine-aspartic acid peptide (RGD)-conjugated d-alpha-tocopheryl polyethylene glycol 1000 succinate (TPGS) mixed micelles (VeC/T-RGD MMs) to deliver BU to ovarian cancer cells to inhibit intraperitoneal metastasis. Moreover, the toxicity of BU was reduced by coating it with the mixed micelles to increase its biocompatibility for practical applications.

Results: The BU-loaded VeC/T-RGD MMs (BU@MMs) had an average diameter of 161 ± 1.4 nm, a zeta potential of 4.49 ± 1.54 mV and a loading efficiency of 2.54%. The results showed that these micelles inhibited cell proliferation, induced apoptosis, and reduced the migration and invasion of A2780 and SKOV3 cells. Further studies indicated that BU@MMs enhanced the levels of E-cadherin and decreased the expression levels of N-cadherin, vimentin and Snail in vitro. In addition, the mixed micelles effectively enhanced the anticancer effect and inhibited intraperitoneal metastasis in intraperitoneal metastatic models. The BU@MMs exhibited fewer toxic side effects than BU, indicating better biocompatibility and biosafety for in vivo applications.

Conclusions: Our studies show that BU@MMs are a potential multifunctional nanodrug delivery system that can effectively inhibit the intraperitoneal metastasis of ovarian cancer.

Keywords: Bufalin, Ovarian cancer, Mixed micelles, Intraperitoneal metastasis, EMT pathway

Background

Ovarian cancer is a high-risk disease that seriously threatens the physical and mental health of women worldwide. Annually, there are 313,959 new ovarian cancer cases and 207,252 deaths globally (Sung et al. 2021). According to the data released by GLOBOCAN, the incidence of ovarian cancer exceeded 8.4/100,000 in 2018 and ranked as the 8th most prevalent cancer in women. The mortality rate is 5.4/100,000, ranking 7th among women. (Lheureux et al. 2019) Taking the high incidence rate in the United States as an example, the mortality rate of ovarian cancer ranks fifth. (Siegel et al. 2021) The main reason for the high mortality of ovarian cancer is tumor cell metastasis, especially in the intraperitoneal cavity.

Currently, ovarian cancer treatment mainly involves surgery and chemotherapy supplemented by maintenance therapy. (Armstrong et al. 2021) Many advanced methods have been applied for maintenance treatment, such as bevacizumab, which is used for antiangiogenic therapy (Pignata et al. 2021); olaparib, which is used as a PARP inhibitor (Friedlander et al. 2021; Poveda et al. 2021); and nivolumab, which can enhance the antitumor activity of T cells by blocking cancer cell immune escape. (Hamanishi et al. 2021) Despite these advanced treatments, the survival rate of patients with ovarian cancer has not improved significantly. (Zeng et al. 2018; Torre et al. 2018) As most patients with ovarian cancer are diagnosed at advanced stages, the tumors are difficult to thoroughly resect due to metastasis, and the patients cannot tolerate chemotherapy well because of its profound adverse effects. (Menon et al. 2021; Kuroki and Guntupalli 2020).

As research has progressed, increasing evidence suggests that the invasion and metastasis of ovarian cancer cells are associated with epithelial-to-mesenchymal transition (EMT), which is characterized by the loss of cell adhesion and the acquisition of migratory and invasive phenotypes. (Fan et al. 2020; Liang et al. 2018a, b; Liang et al. 2018a, b; Nieto et al. 2016; Bakir et al. 2020) Snail induces EMT by downregulating the adhesion protein E-cadherin, driving tumor cells to adopt the mesenchymal phenotype while losing epithelial polarity, as indicated by elevated vimentin and N-cadherin expression. (Pan et al. 2020; Shibue and Weinberg 2017; Pastushenko and Blanpain 2019) In addition, ovarian cancer cells can secrete matrix metalloproteinases (MMPs) to degrade the extracellular matrix (ECM), disrupting the histological barrier and contributing to angiogenesis. All of these effects can induce the invasion and metastasis of ovarian cancer cells. (Qian et al. 2020; Chen et al. 2021a, b, c; Pietila et al. 2021) For example, reducing the protein levels of MMP-2 and MMP-9 in OVCAR-8 and SKOV3 cells can lead to decreased cell migration. (Lu et al. 2020; Liao et al. 2018; Pipaliya et al. 2021) Thus, a novel methodology to effectively inhibit metastasis would be beneficial to all patients with advanced ovarian cancers.

In recent years, the therapeutic applications of traditional Chinese medicines in ovarian cancer have gradually attracted much attention. (Chan et al. 2020; Wang et al. 2019) Bufalin, one of the effective pharmacological components of toad venom, a valuable traditional Chinese medicine, is derived from the secretion of the *Bufo gargarizans* posterior ear gland and epidermal gland. (Yang et al. 2021a, b) Previous studies have shown that BU exerts broad-spectrum antitumor effects. It can inhibit the proliferation of tumor cells, inhibit angiogenesis, induce apoptosis, stimulate cell differentiation, enhance tumor cell autophagy and reverse multidrug resistance. (Xu et al. 2021; Chen

et al. 2021a, b, c; Zhang et al. 2019, 1992; Li et al. 2021) More importantly, it has been reported that BU can inhibit tumor metastasis through the EMT pathway in hepatocellular carcinoma and gastric cancers. (Wang et al. 2016; Zou et al. 2021) Recently, it has been reported that BU can inhibit the migration of PA-1 and OAW28 ovarian cancer cells. (Su et al. 2021) In our preliminary experiment, we found that BU can also inhibit the migration and invasion of A2780 and SKOV3 ovarian cancer cells. However, poor water solubility, high toxicity and imprecise targeting restrict the applications of BU in cancer treatment.

Powered by the rapid development of nanotechnology, significant advances have been made in nanomaterials for cancer treatment over the past two decades. (de Lazaro and Mooney 2021; Rashidi et al. 2016; Guo et al. 2021; Pandey et al. 2022) For example, the development of copper–cysteamine nanoparticles for use in X-ray-induced PDT to microwave-induced PDT has taken only three years. (Shrestha et al. 2019; Zhou et al. 2022) Nanomaterials have significant advantages in tumor treatment due to their adjustable size, diverse functions and good biocompatibility. Studies have shown that nanomaterials with a particle size of 100–200 nm can passively accumulate at a tumor site through the enhanced permeability and retention effect. Alternatively, by integrating packages consisting of certain targeting molecules or ligands, nanomaterials can actively target tumor sites. (Shi and Lammers 2019; Guo et al. 2021; Shi et al. 2017; Perry et al. 2017) Therefore, combining nanomaterials with BU may overcome the drawbacks of BU and could lead to the realization of its promising antitumor effects. (Xu et al. 2021; Gao et al. 2021a, b) In this study, we used VeC/T-RGD MMs (MMs) as a system to deliver BU. In the MMs, VES can encapsulate the insoluble drug, improve encapsulation efficiency and induce tumor cell apoptosis. (Liang and Qiu 2021; Chen et al. 2021a, b, c) As a mitochondriotropic substance, TPGS can endow BU@MMs with mitochondrial-targeting capability. (Assanhou et al. 2015) In addition, RGD can specifically bind to integrin αvβ3 highly expressed in ovarian cancer. (Ahmad et al. 2021) Our previous studies confirmed that BU@MMs can effectively improve antitumor activity in drug-resistant colon cancer. (Yuan et al. 2018) Here, we aim to investigate whether BU@MMs can effectively inhibit the metastasis of ovarian cancers. To this end, we proved that BU@MMs can effectively inhibit ovarian cancer cells in vitro and affect the expression of EMT-related proteins. Furthermore, we established a mouse model of intraperitoneal metastasis to evaluate both the effects of BU@MMs on the intraperitoneal metastasis of ovarian cancer cells and their biosafety.

Results

Preparation, characterization, toxicity and cellular uptake of BU@MMs

The emulsification-solvent evaporation method was used to prepare the BU@MMs (Fig. 1). The specific preparation method can be found in our previous articles. (Yuan et al. 2018) We confirmed the formation of the material by 1H-NMR (Additional file 1: Figure S1) to ensure proper synthesis. The signals at 2.5 − 3.0 ppm belongs to the monosuccinate in TPGS-SA, and methylene appeared at 2.5−3.0 ppm belongs to the succinimide in TPGS-NHS. The signals at 7.0−7.3 ppm belongs to the hydrogen in the benzene ring in RGD. These observations indicated that the TPGS-RGD were successfully synthesized. The physicochemical properties are summarized in Table 1. The particle size of

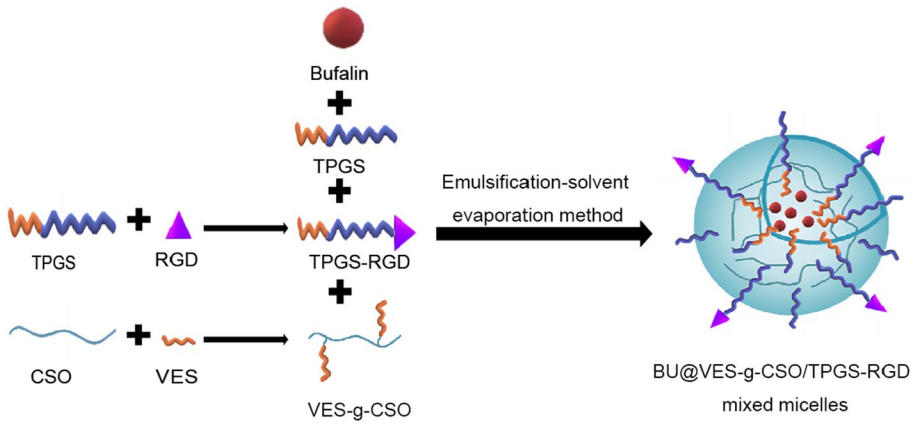

Fig. 1 BU@MMs formulation mechanism

Table 1 Physicochemical properties of BU-loaded mixed micelles

Formulation	VES-g-COS/TPGS/TPGS-RGD (w/w)	LE (%)	Size (nm)	Zeta potential (mV)	PDI
BU@VeC	10/0/0	1.42	162 ± 2.4	33.1 ± 1.72	0.22
BU@VeC/T	10/2/0	2.56	158 ± 1.5	5.41 ± 1.11	0.16
BU@VeC/T-RGD	10/1.76/0.24	2.54	161 ± 1.4	4.49 ± 1.54	0.17

Data are presented as the mean ± SD ($n = 3$)

LE loading efficiency; *PDI* polydispersity index; *BU@VeC* BU-loaded VES-CSO; *BU@VeC/T* BU-loaded VES-CSO/TPGS; *BU@VeC/T-RGD* BU-loaded VES-CSO/TPGS-RGD

the BU@MMs was 161 ± 1.4 nm, the zeta potential was 4.49 ± 1.54 mV, and the loading efficiency (LE) was 2.54%. The particle size of the BU@MMs is smaller than that of the BU-loaded VES-CSO (BU@VeC) because the hydrophobic fragments of TPGS are the same as those of VES, and they were embedded into the cores of the mixed micelles to encapsulate the drugs more tightly. In contrast, after conjugation with RGD, the particle size of the BU@MMs was larger than that of BU-loaded VES-CSO/TPGS (BU@VeC/T) because a portion of the TPGS was combined with RGD, resulting in a reduction in the TPGS content and a slightly loosened structure. The transmission electron microscopy (TEM) image showed that the BU@MMs are spherical in shape with a uniform dispersion (Fig. 2a, b) and a relatively narrow polydispersity index (PDI = 0.17). The BU@MMs maintained their original diameters during stability testing, indicating that BU@MMs have satisfactory stability as a result of the compacted inner core, which is composed of VES-g-CSO and TPGS (Additional file 1: Figure S2a). Moreover, the release profiles of BU from the BU@MMs are shown in Additional file 1: Figure S2b. The performance of these BU-loaded mixed micelles is in accordance with our previous studies.

Toxicity of BU@MMs was examined in human umbilical vein endothelial cells (HUVECs). Results showed that BU@MMs did not have any toxicity in HUVECs (Additional file 1: Figure S3). To observe the cellular uptake of the different formulations of mixed micelles, we replaced BU with coumarin-6 (C6) and carried out a cellular uptake study with SKOV3 cells by CLSM (Fig. 2c, d). After 2 h of incubation, the rate of C6@VeC/T-RGD uptake was significantly higher than that of free C6, C6@VeC or C6@

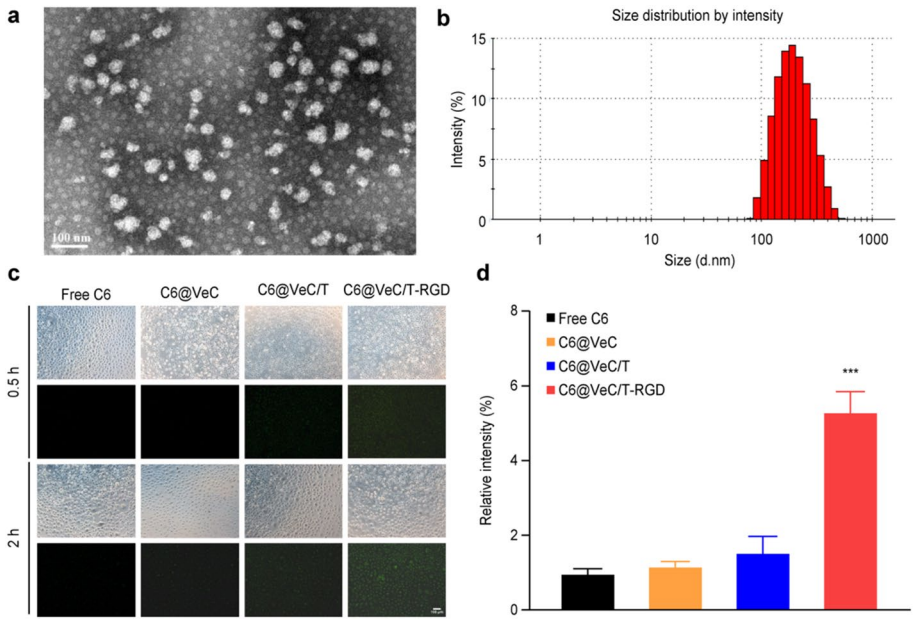

Fig. 2 Characterization and cellular uptake of BU-loaded mixed micelles. **a**, **b** TEM image and particle size distribution of BU@MMs. **c** Uptake by SKOV3 cells after 0.5 h and 2 h of incubation with free C6, C6-labeled VeC mixed micelles, C6-labeled VeC/T mixed micelles, and C6-labeled VeC/T-RGD mixed micelles examined by CLSM. **d** Quantified fluorescence intensity of SKOV3 cellular uptake after 2 h of incubation with free C6, C6-labeled VeC mixed micelles, C6-labeled VeC/T mixed micelles, and C6-labeled VeC/T-RGD mixed micelles. green: C6. Bar: 100 μm. The data are presented as the mean ± SD ($n = 3$). ***$P < 0.001$ indicates statistical significance compared with the control

VeC/T. These results suggested that RGD-targeted mixed micelles increased the cellular uptake capacity and enhanced cancer cell targeting. Hence, these results indicate that we successfully prepared BU@MMs with a suitable particle size and narrow size distribution, and they showed high uptake by ovarian cancer cells.

Inhibitory effect of BU@MMs on ovarian cancer cells in vitro

To explore the inhibitory effects of BU, MMs and BU@MMs, cell proliferation was monitored by CCK-8 assay, and BU@MMs inhibited A2780 and SKOV3 cell proliferation better than free BU. The results show that the half-maximal inhibitory concentrations (IC_{50} values) of the BU@MMs in A2780 and SKOV3 cells were 0.57 ± 0.06 ng/ml and 2.14 ± 0.14 ng/ml, respectively (Fig. 3a, b). In addition, the IC_{50} values of BU in A2780 and SKOV3 cells were 7.62 ± 0.35 ng/ml and 10.84 ± 0.14 ng/ml, respectively. Therefore, BU@MMs are expected to inhibit the proliferation of ovarian cancer cells in vitro better than free BU due to their greater solubility and increased cellular uptake.

To determine whether BU@MMs can effectively promote the apoptosis of ovarian cancer cells, we performed flow cytometry analysis with A2780 and SKOV3 ovarian cancer cells. The results showed that the apoptosis rates of A2780 and SKOV3 cells were affected by the treatments in descending order as follows: BU@MMs > BU > MMs > Ctrl (Fig. 3c–f). BU@MMs showed the strongest effect on apoptosis induction in ovarian cancer cells. Moreover, we examined the expression of apoptosis-related proteins, including bcl-2, bax, cleaved caspase-3 and cleaved caspase-9, by Western blotting.

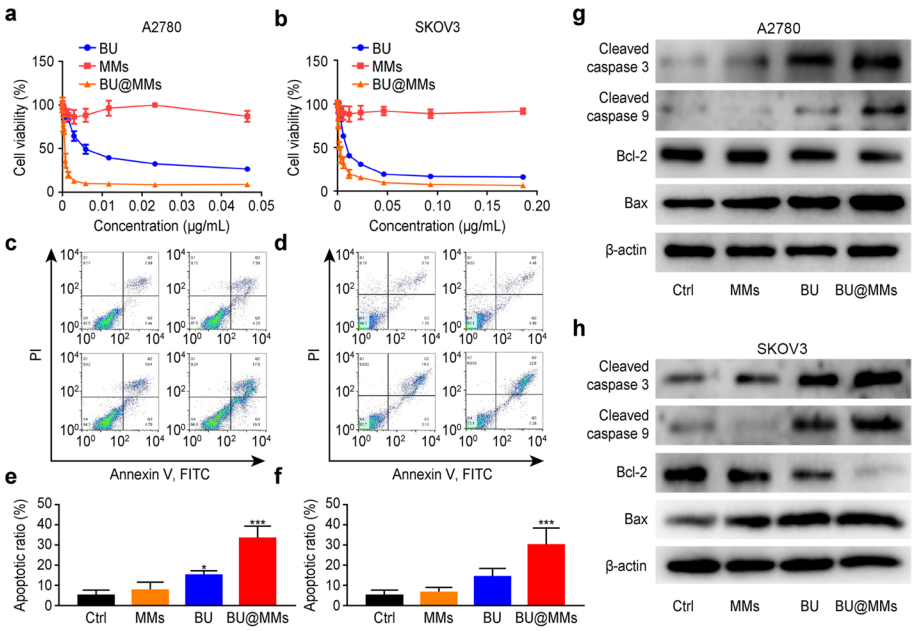

Fig. 3 Effect of BU@MMs on the proliferation and apoptosis of A2780 and SKOV3 cells. **a**, **b** The viability of A2780 and SKOV3 cells after incubation with BU, MMs and BU@MMs analyzed by CCK-8 assay. The apoptotic rates of A2780 (**c**) and SKOV3 (**d**) cells after incubation with BU, MMs, and BU@MMs evaluated by flow cytometry. Untreated cells were used as controls. Bar charts showing the average apoptotic ratio of A2780 (**e**) and SKOV3 (**f**) cells. Western blotting was performed to detect the protein expression of bcl-2, bax, cleaved caspase-3 and cleaved caspase-9 in A2780 (**g**) and SKOV3 (**h**) cells. The data are presented as the mean ± SD ($n = 3$). $^{*}P < 0.05$, $^{***}P < 0.001$ indicate statistical significance compared with the control

We observed that the expression levels of the proapoptotic molecules bax, cleaved caspase-3, and cleaved caspase-9 were increased after BU@MM treatment compared with the effect of free BU, while the expression level of the antiapoptotic molecule bcl-2 was decreased in both A2780 and SKOV3 cells (Fig. 3g, h). Our study proved that BU induced ovarian cancer cell apoptosis and that BU@MMs increased the apoptosis rate to an extent greater than that of free BU.

In addition, as shown in Fig. 3a–h, the blank MMs exerted no effects on cell proliferation, apoptosis or the expression of apoptosis-related proteins. Therefore, it can be preliminarily proven that the blank MMs are nontoxic.

In conclusion, BU@MMs inhibited the proliferation and promoted the apoptosis of ovarian cancer cells in vitro.

BU@MMs inhibit ovarian cancer cell migration and invasion through the EMT pathway

The effects of BU@MMs on the migration and invasion of ovarian cancer cells were evaluated by transwell assays and tube formation assays, as migration and invasion are keys to tumor metastasis. The transwell assay proved that, compared to the other groups, the BU@MMs prominently decreased the migration and invasion of A2780 and SKOV3 cells (Fig. 4a–h). To further demonstrate the antimetastatic effect of BU@MMs on ovarian cancer, we performed a tube formation assay with human umbilical vein endothelial cells (HUVECs), as angiogenesis plays an important role in tumor metastasis. The invasion and metastasis of tumor cells depend on sufficient angiogenesis and blood supply, and

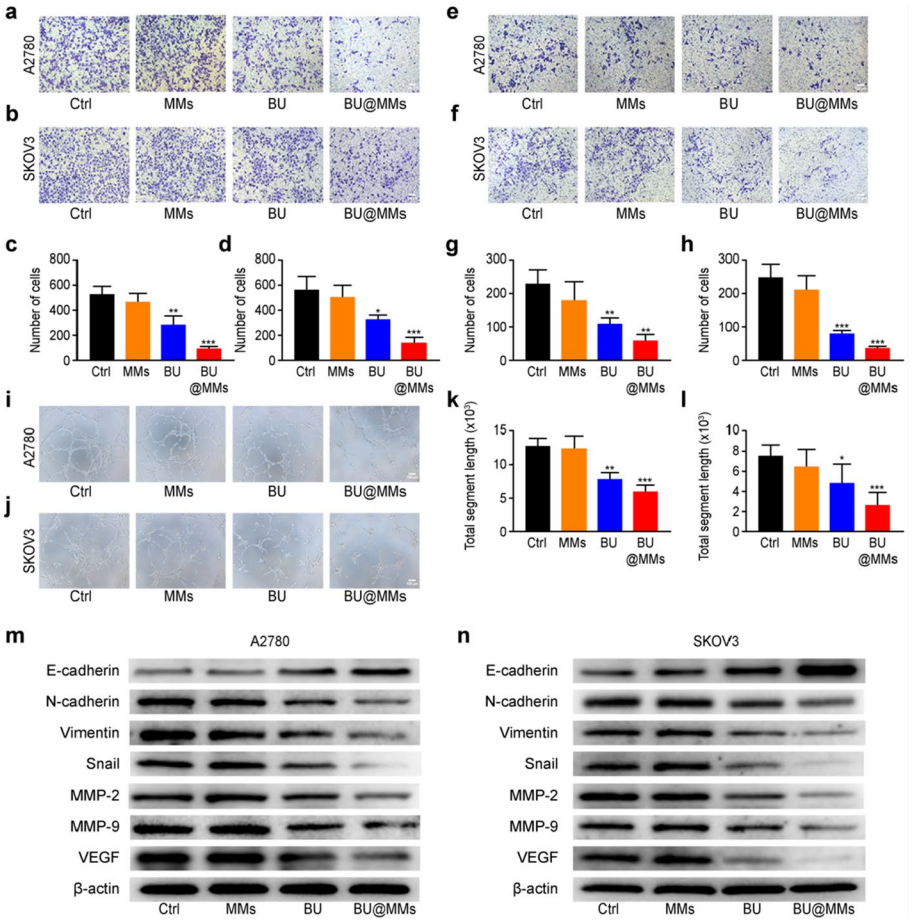

Fig. 4 Effects of BU@MMs on the migration and invasion of A2780 and SKOV3 cells. **a**, **b** Representative images of migrating A2780 and SKOV3 cells. Bar charts showing the number of migrating A2780 (**c**) and SKOV3 (**d**) cells. **e**, **f** Representative images of the invasion of A2780 and SKOV3 cells. Bar charts showing the number of invaded A2780 (**g**) and SKOV3 (**h**) cells. **i**, **j** Tube formation by HUVECs cultured on Matrigel compared to the tube formation by A2780 and SKOV3 cells. Bar charts showing the total segment lengths in A2780 (**k**) and SKOV3 (**l**) cells. Expression of proteins related to the EMT pathway in A2780 (**m**) and SKOV3 cells (**n**), including E-cadherin, N-cadherin, vimentin, Snail, MMP-2, MMP-9 and VEGF. Bar: 100 μm. Data are presented as the mean ± SD ($n = 3$). *$P < 0.05$, **$P < 0.01$ and ***$P < 0.001$ indicate statistical significance compared with the control

angiogenesis depends on the balance of regulatory factors such as VEGF. Figure 4i–l shows that, compared with the Ctrl, MMs and BU, BU@MMs decreased the lumen length and continuity of the tubes formed by HUVECs.

Moreover, to verify whether BU@MMs can inhibit the migration and invasion of ovarian cancer cells through the EMT pathway, we detected the expression of proteins related to this pathway by Western blotting. The results showed that, compared with free BU, BU@MMs enhanced the levels of E-cadherin but decreased the expression levels of N-cadherin, vimentin and Snail in both A2780 and SKOV3 cells, while the Ctrl and MMs groups showed no significant effects on EMT markers. In addition, the expression levels of MMP-2 and MMP-9, which are associated with ECM degradation, and VEGF, which is related to increased vascular growth, were also decreased in the BU@MM group (Fig. 4m, n).

All these results show that BU@MMs can effectively inhibit the migration and invasion of ovarian cancer cells through the EMT pathway.

BU@MMs inhibit ovarian cancer intraperitoneal metastasis in vivo

Intraperitoneal metastasis is the most common pathway of ovarian cancer metastasis. To determine whether BU@MMs can effectively inhibit intraperitoneal metastasis in vivo, we established an ID8 cell intraperitoneal metastasis model in female C57BL/6 mice (Fig. 5a). Compared with the Ctrl, BU effectively inhibited ovarian cancer intraperitoneal metastasis, and BU@MMs showed a greater inhibitory effect than BU. Specifically, mice with intraperitoneal metastasis showed significant increases in abdominal circumference and ascites volume. BU@MMs inhibited abdominal circumference by 28.16% and ascites volume by 84.81%, both of which were markedly higher than the respective 18.61% and 66.47% reductions induced by free BU (Fig. 5b, c, k). In addition, we observed that the color of the ascites in the BU@MM group was significantly lighter than that in the saline group, in which the ascites were bloody (Fig. 5j). Furthermore, there was no evident difference in mouse body weight between the BU@MMs and the free BU groups, indicating that our MMs induced no toxic side effects in mice (Fig. 5d). Thus, BU@MMs effectively inhibited the formation of ascites in the ovarian cancer intraperitoneal metastasis model.

Our results displayed in Fig. 5e–i show that there were fewer metastatic tumor nodules in the intraperitoneal cavities of the animals in the BU@MM group, including on the abdominal wall, intestine and diaphragm, than in the other three groups (Ctrl, MMs and BU), especially intestinal metastases (Fig. 5h, l). BU@MMs more effectively inhibited the formation of metastatic ovarian tumor nodules in the intraperitoneal cavity.

Moreover, we evaluated the antimetastatic effects by measuring the concentrations of MMP-2, MMP-9, and VEGF in mouse serum. Their concentrations were the lowest in the BU@MM group, which is consistent with the in vitro observations (Fig. 5m–o).

All of these results indicate that BU@MMs can effectively inhibit the intraperitoneal metastasis of ovarian cancer in vivo.

Biosafety evaluations of BU@MMs in vivo

To evaluate the biosafety of the BU@MMs, histopathological analysis was performed on the main organs of the mice, including the heart, liver, spleen, lung and kidney. As shown in Fig. 6, BU caused varying degrees of damage to the main organs, especially the myocardial tissue; in stark contrast, BU@MMs caused almost no damage to these organs. These results indicate that the BU@MMs produce substantially fewer toxic side effects than BU and that the conjugated TPGS mixed micelles improved the biocompatibility and biosafety of BU@MMs.

Discussion

Ovarian cancer produces malignant tumors and has a low survival rate and a high recurrence rate. The difficulty in ovarian cancer treatment is due to metastasis to the intraperitoneal cavity. It is commonly believed that ovarian cancer metastasizes through the EMT pathway. (Mitra et al. 2017) EMT is a complex process in which the adhesion between tumor cells is lost, the cells acquire pre- and postpolarity, and the ECM

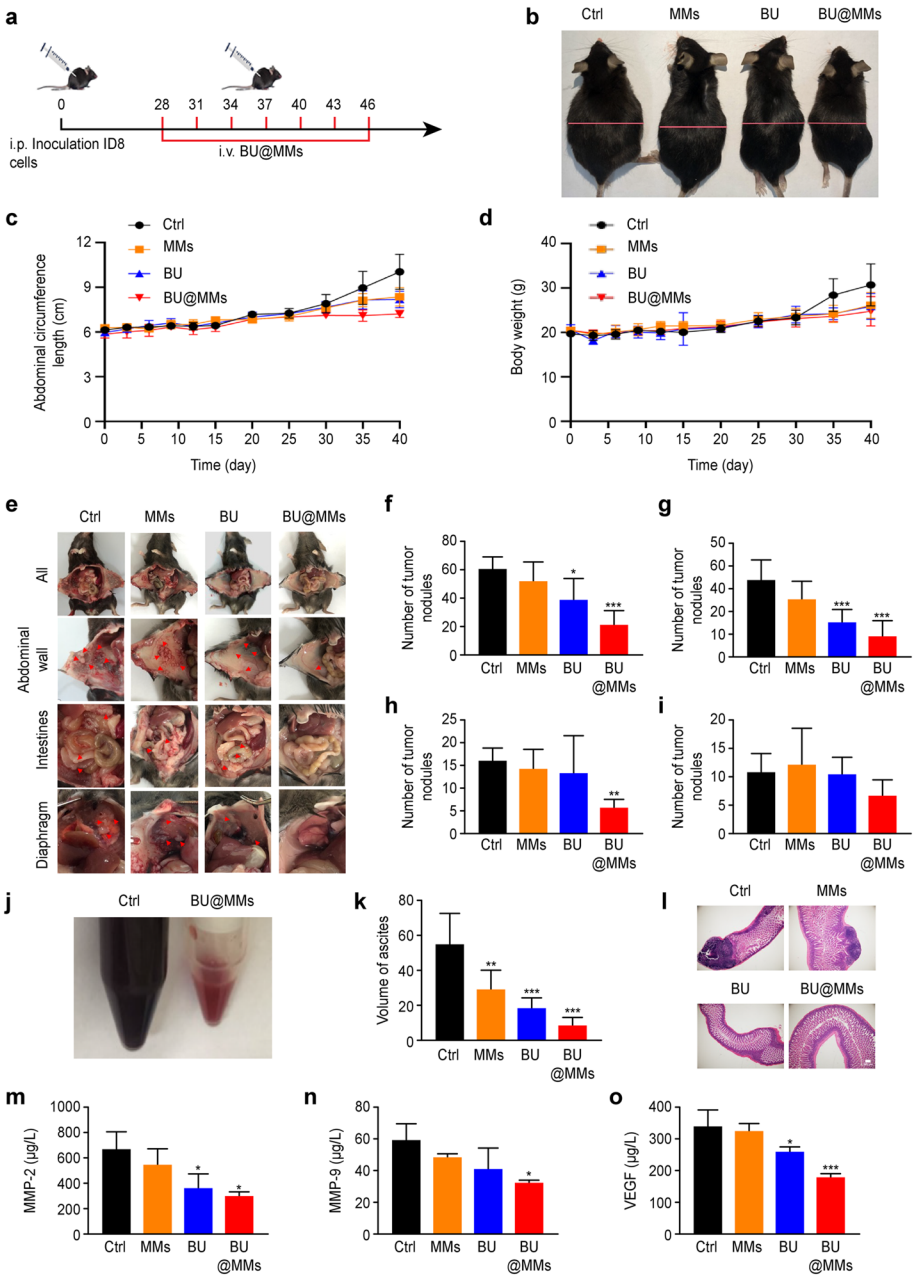

Fig. 5 Inhibitory effect of BU@MMs on ovarian cancer intraperitoneal metastasis in vivo. **a** The timeline of the animal experiment. **b** Representative images of the abdominal circumferences of the mice on the 40th day. **c, d** Abdominal circumferences and body weights during the period of treatment. **e** Representative images of metastatic tumor nodules from the intraperitoneal cavity. The number of metastatic tumor nodules in the intraperitoneal cavity (**f**), including the abdominal wall (**g**), intestines (**h**), and diaphragm (**i**). **j** The color of the ascites in the BU@MMs and Ctrl groups. **k** Ascites volume. **l** H&E-stained histological images of mouse intestines from various groups. The concentrations of MMP-2 (**m**), MMP-9 (**n**), and VEGF (**o**) in mouse serum. Bar: 200 μm. The data are presented as the mean ± SD ($n = 6$). *$P < 0.05$, **$P < 0.01$ and ***$P < 0.001$ indicate statistical significance compared with the control

is altered (Nieto et al. 2016; Lambert and Weinberg 2021). Thus, ovarian cancer cells acquire the ability to migrate and invade. Effectively inhibiting ovarian cancer metastasis would be a good solution to help prolong the survival of patients with ovarian cancers.

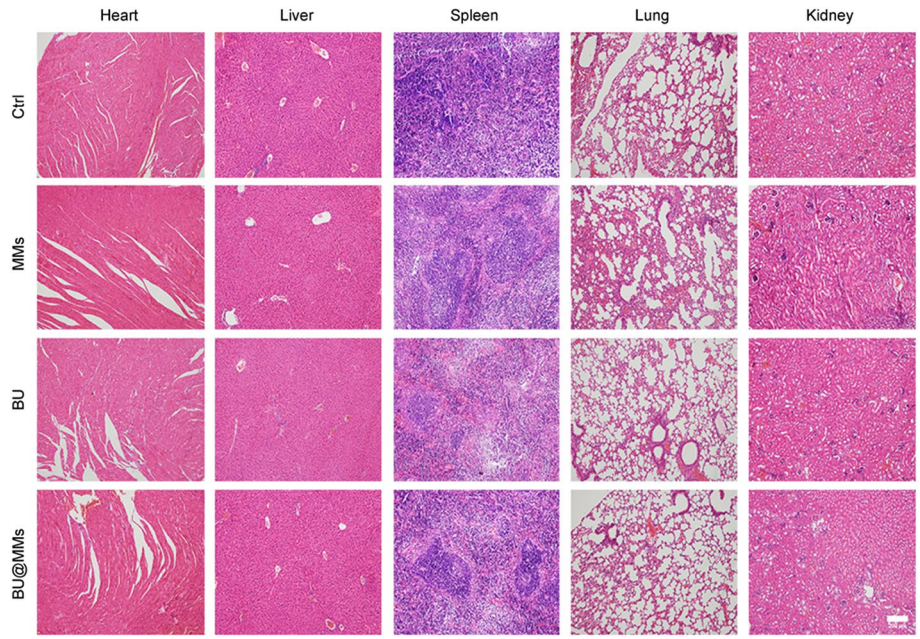

Fig. 6 H&E-stained histological images of the main organs (heart, liver, spleen, lung and kidney) from the animals in various groups. Bar: 200 μm

BU, an effective antitumor pharmacological component of the traditional Chinese medicine Chansu, can effectively inhibit the invasion and metastasis of certain tumor cells, such as gastric cancer and hepatocellular carcinoma, through the EMT pathway. (Wang et al. 2016; Zou et al. 2021) However, whether BU can effectively inhibit ovarian cancer metastasis through the EMT pathway is still unknown. Moreover, due to its toxicity, insolubility, rapid metabolism and short half-life, the applications of BU for cancer treatment are limited. (Gao et al. 2021a, b; Yang et al. 2021a, b) Accordingly, multiple nanodelivery systems have been investigated for loading BU to achieve precise targeting, enhance its antitumor effects, reduce its toxicity, and prolong its half-life (Hu et al. 2020; Zeng et al. 2021).

In this study, we prepared BU@MMs to improve the inhibitory effect of BU on ovarian cancer and to reduce its toxicity and side effects. The characterization of BU@MMs is shown in Table 1, Fig. 2 and Additional file 1: Figures S1-3, and we observed that the mixed micelles were an ideal drug delivery system for BU, as they can greatly increase the cellular uptake of BU. Such high uptake is attributed to the conjugation of RGD and TPGS, as RGD can be specifically recognized by the highly expressed integrin αvβ3 on the surface of ovarian cancer cells; therefore, targeting integrin αvβ3 may enable more efficient drug delivery to ovarian cancer cells. Moreover, TPGS can further enhance uptake by reducing drug efflux and promoting NP circulation. Compared to free BU and MMs, BU@MMs more effectively inhibited the proliferation and promoted the apoptosis of ovarian cancer cells (Fig. 3). Furthermore, BU@MMs effectively inhibited the migration and invasion of ovarian cancer cells through EMT and inhibited angiogenesis, which is essential for metastasis. Changes in the expression levels of E-cadherin, N-cadherin, vimentin and Snail, which are related to EMT,

and MMP-2 and MMP-9, which are related to the ECM, were observed (Fig. 4). In the mouse model of intraperitoneal metastasis established with ID8 cells, BU@MMs showed superior inhibition of ovarian cancer cell metastasis and demonstrated good biocompatibility and biosafety (Figs. 5, 6). These results were mainly attributed to the MMs increasing the solubility and targeting of BU while reducing its toxicity.

As mentioned above, bufalin has a significant antitumor effect in a variety of tumors. However, due to high toxicity, poor water solubility, fast metabolism, short half-life, its application is seriously limited in cancer therapy. The formation of nano-carriers is an effective way to improve the therapeutic effect of bufalin. Several studies have taken advantage of nano-drug delivery systems to target delivery of bufalin for enhance its antitumor therapy and attenuate toxicity, such as platelet membrane biomimetic nanoparticle, liposomes, polymeric prodrug, bovine serum albumin nanoparticle, monodisperse mesoporous silica nanoparticle, metal–organic frameworks(MOFs) and so on (Tian et al. 2014; Ning et al. 2022; Zeng et al. 2021; Hu et al. 2012; Wen et al. 2017; Ettlinger et al. 2022). Zeng et al. designed pH-sensitive and redox-responsive folic acid-modified MOFs as drug carriers of bufalin (FA-MOF/Buf), which could improve water solubility and stability, higher intracellular uptake, and enhanced antitumor effect of bufalin in breast cancer (Zeng et al. 2021). Ning et al. prepared a monodisperse mesoporous silica nanoparticle to load lenvatinib and bufalin for targeted delivery to cholangiocarcinoma, which indicated a superior therapeutic effect than free drugs (Ning et al. 2022). Compared with previously reported nano-drug delivery systems, VES-CSO/TPGS-RGD MMs are easier to prepare and more multifunctional. As a water-soluble derivative of vitamin E, VES can encapsulate insoluble BU. TPGS can enhance circulation, target the mitochondria and resist drug resistance. RGD can specifically bind to integrin receptor αvβ3 in ovarian cancer and play active targeting effect. CSO can further improve the solubility and stability of the drug. VES-CSO and TPGS-RGD can self-assemble in water, RGD, conjugates onto the surface of these mixed micelles. Nevertheless, this nanodelivery system will be further optimized in our future study.

Clinically, during chemotherapy for ovarian cancer, platinum drugs can cause serious renal function impairment, leading to treatment interruption, which might easily lead to treatment failure. BU@MMs showed almost no damage to vital organs, including the kidney, and exhibited better biocompatibility and biosafety than BU alone. This platform inherits the excellent antitumor effect of bufalin plus the special effect of inhibiting intraperitoneal metastasis and overcomes the disadvantage of high toxicity for use in clinical applications. Our studies suggest that the use of BU@MMs can provide a new solution for the clinical treatment of ovarian cancer, which causes malignant tumors and has a low survival rate.

Conclusion

In this study, we successfully designed BU@MMs to inhibit intraperitoneal metastasis of ovarian cancer. In vitro experiments clearly proved that BU@MMs exerted stronger effects than free BU in inhibiting tumor cell proliferation, promoting tumor cell apoptosis, and inhibiting tumor cell migration and invasion through the EMT pathway in A2780 and SKOV3 ovarian cancer cells. In vivo experiments confirmed that BU@MMs

more effectively inhibit the intraperitoneal metastasis of ovarian cancers. In addition, BU@MMs have very low toxicity and do not cause any damage to important organs. Therefore, BU@MMs are a potential multifunctional nano-drug delivery system that can effectively inhibit the intraperitoneal metastasis of ovarian cancer to provide effective treatment.

Materials and methods

Materials

BU was provided by Chengdu Herbpurify Co., Ltd. (Sichuan, China). C6 was obtained from Sigma-Aldrich Chemical Co. (St. Louis, MO, USA). CSO (MW 5 kDa, 90.0% deacetylation degree) was provided by Aoxing Co., Ltd. (Zhejiang, China). VES was purchased from TCI Development Co., Ltd. (Shanghai, China). TPGS and c(RGDfK) were provided by GL Biochem Ltd. (Shanghai, China). All other solvents were of analytical grade. Phosphate-buffered saline (PBS), fetal bovine serum (FBS), and RPMI-1640 medium were sourced from Gibco BRL (Carlsbad, CA, USA). CCK-8 was obtained from Dojindo (Kumamoto, Japan). An Annexin V-FITC apoptosis detection kit was provided by BD Biosciences (Beijing, China). The primary antibodies against cleaved caspase-3, cleaved caspase-9, bcl-2, bax, E-cadherin, and MMP-9 and the secondary antibodies were from Cell Signaling Technology (Boston, MA, USA). Primary antibodies against N-cadherin, vimentin, Snail, MMP-2, VEGF and β-actin were purchased from Abcam (Cambridge, UK). Mouse MMP-2, MMP-9 and VEGF ELISA kits were from JingMei Bioengineering Company (Shenzhen, China).

Cells lines and mice

A2780 human ovarian cancer cells were purchased from Jiadeno Biotechnology Co., Ltd. (Shanghai, China). SKOV3 human ovarian cancer cells and ID8 mouse ovarian cancer cells were gifts from Ruixin Wu (Shanghai University of Traditional Chinese Medicine). All cells were cultured in RPMI-1640 medium supplemented with 10% FBS and penicillin/streptomycin, and all were maintained at 37 °C in a humidified atmosphere with 5% CO_2.

HUVECs (ScienCell, USA) were cultured in endothelial cell medium (ScienCell, USA), and only early passages (< p6) were used.

Female C57BL/6 mice (6–8 weeks old, Shanghai SLAC Laboratory Animal Co. Ltd.) were used to establish intraperitoneal metastasis models. The animal study was reviewed and approved by the Administrative Panel on Laboratory Animal Care of the Putuo District Central Hospital. All animal experiments were performed in accordance with the Guide for the Care and Use of Laboratory Animals.

Preparation and characterization of BU@MMs

VeC/T-RGD MMs, BU@VeC, BU@VeC/T and BU@MMs were prepared by organic solvent emulsification–evaporation as described, except that BU (1 mg) was separately contained in 200 μL of chloroform. Excess unentrapped BU was removed by passage through a 0.45 μm filter. The average particle size, zeta potential and PDI of the BU@MMs were examined by a Malvern Zetasizer Nano ZS90 DLS (Malvern

Instruments, Malvern, UK). A transmission electron microscope (JEM-2100; JEOL, Tokyo, Japan) was used to determine the surface morphology of BU@MMs.

To determine the drug loading amount (LA), BU-loaded mixed micelles were first diluted with methanol. After the samples were vortexed and sonicated, 20 μL of the supernatant was injected into an HPLC system (Agilent 1260 Infinity, Agilent, Japan) to analyze the BU concentration. Finally, the LE of the BU in the mixed micelles was calculated as

$$LE = \frac{BU\ loaded\ amount\ (LA)}{total\ BU\ added\ during\ the\ loading\ procedure} \times 100\%.$$

In vitro cellular uptake of BU@MMs

SKOV3 cells were seeded in a 24-well plate (50,000 cells/well) and maintained with 500 μL of culture medium for 24 h. VeC, VeC/T and VeC/T-RGD were loaded with C6 (500 μg/mL), a fluorescent dye, but not with BU. Then, free C6, C6-labeled VeC, C6-labeled VeC/T and C6-labeled VeC/T-RGD were added to each well containing RPMI-1640 (final volume: 500 μL) and incubated for 0.5 or 2 h at 37 °C. The cells were washed twice with PBS at the end of the incubation period, and images were acquired by CLSM (Leica, Heidelberg, Germany).

Cell proliferation assay

The inhibitory effects of BU, MMs and BU@MMs on the proliferation of A2780 and SKOV3 cells was assessed by CCK-8 assay. A2780 or SKOV3 cells were seeded in a 96-well plate at a density of 1×10^4 cells/well and cultivated at 37 °C. After 24 h, the medium was replaced with medium containing BU, MMs, or BU@MMs at the same concentration (0–0.0465 μg/mL for A2780 cells and 0–0.186 μg/mL for SKOV3 cells), and the cells were incubated for 48 h. At the end of treatment, the viability of the cells was analyzed by CCK-8 assay according to the instructions of the kit manufacturer. Following these same steps, cells were seeded in a 6-well plate at a density of 2×10^5 cells/well, and the medium was collected and used as conditioned medium for tubule formation, migration and invasion assays.

Flow cytometric apoptosis assay

The effects of BU, MMs and BU@MMs on A2780 and SKOV3 cell apoptosis was assessed by a flow cytometric apoptosis assay. A2780 or SKOV3 cells (2×10^5 cells/well) were seeded in 6-well plates and cultured for 24 h. After reaching 80% confluence, the cells were incubated with BU, MMs, or BU@MMs for 48 h. In addition, cell suspensions at a density of 1×10^6/mL were diluted with 100 μl of binding buffer. Then, 5 μL of Annexin V-FITC and 5 μL of propidium iodide solution were added for incubation with the cells for 15 min in the dark, followed by immediate analysis using a flow cytometer (BD FACSCanto II; BD Biosciences, San Jose, CA).

Western blot analysis

Total protein was extracted from A2780 and SKOV3 cells using RIPA lysis buffer (Beyotime, China) after the cells were treated with different formulations for 48 h. Protein

samples were separated by SDS-polyacrylamide gel electrophoresis (SDS–PAGE) and transferred to polyvinylidene difluoride membranes. The membranes were blocked in 5% nonfat dry milk in TBST for 1 h at room temperature followed by overnight incubation with the indicated primary antibodies at 4 °C. Then, the blots were incubated with the corresponding horseradish peroxidase-labeled secondary antibodies for 1 h at room temperature, and the bands were visualized using a chemiluminescent ECL assay kit (Merck Millipore).

In vitro *migration and invasion assays*

The cell migration and invasion abilities were evaluated with Transwell chambers (8 μm pore size, Corning). A2780 and SKOV3 cells were seeded in a 6-well plate at a density of 2×10^5 cells/well for 24 h, and the medium was replaced with serum-free medium containing MMs, BU, or BU@MMs as described above and incubated for another 48 h. The conditioned medium was then collected. To assess invasion ability, 8 μm membrane pores coated with 30 μl of basement membrane matrix (BD Biosciences) for 3 h at 37 °C were diluted with blank medium at a ratio of 1:6. Then, 3×10^4 cells for migration assays or 5×10^4 cells for invasion assays in 300 μl of serum-free medium were added to the upper chamber, and the bottom well was filled with 700 μl of complete medium. After 48 h of incubation, the inserts were removed, the cells on the upper side of the inserts were removed by cotton swabs, and the cells on the underside were stained with crystal violet. The cells were observed and photographed under a light microscope.

Tube formation assay

A 96-well plate was coated with 50 μl of ice-cold BD Matrigel. After 30 min, 30,000 HUVECs in 100 μL of conditioned medium were added to the wells. HUVECs were incubated at 37 °C for 4 to 6 h and then visualized by light microscopy. The number of branch points (≥ 3 cells per branch) was counted and analyzed in five random fields per replicate.

Animal models

ID8 cells (5×10^6) in 200 μL of PBS were injected into the intraperitoneal cavity of female C57BL/6 mice. According to the preliminary experimental results, the mice were treated during the 4th week after modeling. The mice were randomly assigned to 4 groups ($n = 6$) and intravenously injected with saline, MMs, BU, or BU@MMs (BU: 0.062 mg/kg). Treatment was repeated 7 times at 3-day intervals. Body weights and tumor growth were monitored regularly. At the end of treatment, all organs (heart, liver, lung, spleen and kidney) and the small intestine were collected for histological analysis.

Enzyme-linked immunosorbent assay (ELISA)

The levels of MMP-2, MMP-9 and VEGF in mouse serum were measured using ELISA kits for mouse MMP-2, MMP-9 and VEGF, and the procedures were performed according to the manual provided by JingMei Bioengineering Company (Shenzhen, China).

Histopathological analysis

Tissues were fixed in 10% formalin, embedded in paraffin, and then sectioned (4 μm thick). Subsequently, slides were stained with hematoxylin and eosin (H&E) following a standard protocol and observed by a microscope (Leica).

Statistical analysis

All data are presented as the mean ± SD. The results were analyzed using GraphPad Prism 8 software, and statistical comparisons were made with one-way ANOVA. Statistical significance was set at $^{*}P < 0.05$, $^{**}P < 0.01$ and $^{***}P < 0.001$.

Abbreviations

BU	Bufalin
VES	Vitamin E succinate
CSO	Chitosan oligosaccharide
RGD	Arginine-glycine-aspartic acid peptide
TPGS	D-Alpha-tocopheryl polyethylene glycol 1000 succinate
VeC/T-RGD MMs	VES-CSO/TPGS-RGD mixed micelles
MMs	VeC/T-RGD MMs
BU@MMs	BU-loaded VeC/T-RGD MMs
EMT	Epithelial-to-mesenchymal transition
MMPs	Matrix metalloproteinases
ECM	Extracellular matrix
LE	Loading efficiency
BU@VeC	BU-loaded VES-CSO
BU@VeC/T	BU-loaded VES-CSO/TPGS
TEM	Transmission electron microscopy
PDI	Polydispersity index
C6	Coumarin-6
IC50	Half-maximal inhibitory concentration
HUVECs	Human umbilical vein endothelial cells
PBS	Phosphate-buffered saline
FBS	Fetal bovine serum
LA	Drug loading amount
SDS-PAGE	SDS-polyacrylamide gel electrophoresis
ELISA	Enzyme-linked immunosorbent assay
H&E	Hematoxylin and eosin
MOFs	Metal–organic frameworks

Supplementary Information

The online version contains supplementary material available at https://doi.org/10.1186/s12645-023-00178-7.

Additional file 1: Figure S1. 1H-NMR spectra of TPGS **(A)**, TPGS-SA **(B)**, TPGS-NHS **(C)** and TPGS-RGD **(D)**. **Figure S2.** Changes of particle size and particle distribution index of BU@MMs in PBS for 7 days at 37℃, measured by dynamic light scattering (a). In vitro BU release curve from BU@MMs in PBS (pH7.4) at 37℃ (b). The data are presented as the mean±SD (n=3). **Figure S3.** Viability of HUVECs treated with BU@MMs for 24 h at 37℃. Note: The data are presented as the mean±SD (n=3).

Acknowledgements
Not applicable.

Author contributions
LX, ZY, and PY conceived and designed the study. LX and SM performed the experiments and data analysis and wrote the manuscript. BF provided valuable suggestions for this study. All authors read and approved the final manuscript.

Funding
We acknowledge the support from the National Nature Science Foundation of China (81973700), the Science and Technology Innovation Project of Shanghai Putuo District Health Commission (ptkwws202004), the project of Putuo Hospital of Shanghai University of Traditional Chinese Medicine (2020370B), the "Xinglin Scholar" of Chengdu University of Traditional Chinese Medicine (YYZX2020123) and the Clinical Specialized Discipline of Health System of Putuo District in Shanghai (2021tszk01).

Availability of data and materials
All data generated or analyzed during this study are included in this published article and its additional information on file.

Declarations

Ethics approval and consent to participate
The animal study was reviewed and approved by the Administrative Panel on Laboratory Animal Care of the Putuo District Central Hospital. All animal experiments were performed in accordance with the Guide for the Care and Use of Laboratory Animals.

Consent for publication
All authors reviewed and agreed with the publication of this manuscript in this journal.

Competing interests
The authors declare that they have no competing interests.

Received: 13 January 2023 Accepted: 17 March 2023
Published online: 27 March 2023

References

Ahmad K, Lee EJ, Shaikh S, Kumar A, Rao KM, Park SY, Jin JO, Han SS, Choi I (2021) Targeting integrins for cancer management using nanotherapeutic approaches: recent advances and challenges. Semin Cancer Biol 69:325–336

Armstrong DK, Alvarez RD, Bakkum-Gamez JN, Barroilhet L, Behbakht K, Berchuck A, Chen LM, Cristea M, DeRosa M, Eisenhauer EL, Gershenson DM, Gray HJ, Grisham R, Hakam A, Jain A, Karam A, Konecny GE, Leath CA, Liu J, Mahdi H, Martin L, Matei D, McHale M, McLean K, Miller DS, O'Malley DM, Percac-Lima S, Ratner E, Remmenga SW, Vargas R, Werner TL, Zsiros E, Burns JL, Engh AM (2021) Ovarian cancer, version 2.2020, NCCN clinical practice guidelines in oncology. J Natl Compr Canc Netw 19:191–226

Assanhou AG, Li W, Zhang L, Xue L, Kong L, Sun H, Mo R, Zhang C (2015) Reversal of multidrug resistance by co-delivery of paclitaxel and lonidamine using a TPGS and hyaluronic acid dual-functionalized liposome for cancer treatment. Biomaterials 73:284–295

Bakir B, Chiarella AM, Pitarresi JR, Rustgi AK (2020) EMT, MET, plasticity, and tumor metastasis. Trends Cell Biol 30:764–776

Chan DW, Yung MM, Chan YS, Xuan Y, Yang H, Xu D, Zhan JB, Chan KK, Ng TB, Ngan HY (2020) MAP30 protein from Momordica charantia is therapeutic and has synergic activity with cisplatin against ovarian cancer in vivo by altering metabolism and inducing ferroptosis. Pharmacol Res 161:105157

Chen D, Li B, Lei T, Na D, Nie M, Yang Y, Xie C, He Z, Wang J (2021a) Selective mediation of ovarian cancer SKOV3 cells death by pristine carbon quantum dots/Cu2O composite through targeting matrix metalloproteinases, angiogenic cytokines and cytoskeleton. J Nanobiotechnol 19:68

Chen J, Wang H, Jia L, He J, Li Y, Liu H, Wu R, Qiu Y, Zhan Y, Yuan Z, Cao Y, Li W, Xu K, Yin P (2021b) Bufalin targets the SRC-3/MIF pathway in chemoresistant cells to regulate M2 macrophage polarization in colorectal cancer. Cancer Lett 513:63–74

Chen X, Gu J, Sun L, Li W, Guo L, Gu Z, Wang L, Zhang Y, Zhang W, Han B, Chang J (2021c) Efficient drug delivery and anticancer effect of micelles based on vitamin E succinate and chitosan derivatives. Bioact Mater 6:3025–3035

De Lazaro I, Mooney DJ (2021) Obstacles and opportunities in a forward vision for cancer nanomedicine. Nat Mater 20:1469–1479

Ettlinger R, Lachelt U, Gref R, Horcajada P, Lammers T, Serre C, Couvreur P, Morris RE, Wuttke S (2022) Toxicity of metal-organic framework nanoparticles: from essential analyses to potential applications. Chem Soc Rev 51:464–484

Fan L, Lei H, Zhang S, Peng Y, Fu C, Shu G, Yin G (2020) Non-canonical signaling pathway of SNAI2 induces EMT in ovarian cancer cells by suppressing miR-222-3p transcription and upregulating PDCD10. Theranostics 10:5895–5913

Friedlander M, Moore KN, Colombo N, Scambia G, Kim BG, Oaknin A, Lisyanskaya A, Sonke GS, Gourley C, Banerjee S, Oza A, Gonzalez-Martin A, Aghajanian C, Bradley WH, Liu J, Mathews C, Selle F, Lortholary A, Lowe ES, Hettle R, Flood E, Parkhomenko E, DiSilvestro P (2021) Patient-centred outcomes and effect of disease progression on health status in patients with newly diagnosed advanced ovarian cancer and a BRCA mutation receiving maintenance olaparib or placebo (SOLO1): a randomised, phase 3 trial. Lancet Oncol 22:632–642

Gao C, Zheng P, Liu Q, Han S, Li D, Luo S, Temple H, Xing C, Wang J, Wei Y, Jiang T, Chen W (2021a) Recent advances of upconversion nanomaterials in the biological field. Nanomaterials 11:2474

Gao L, Zhang L, He F, Chen J, Zhao M, Li S, Wu H, Liu Y, Zhang Y, Ping Q, Hu L, Qiao H (2021b) Surfactant assisted rapid-release liposomal strategies enhance the antitumor efficiency of bufalin derivative and reduce cardiotoxicity. Int J Nanomed 16:3581–3598

Guo J, Yu Z, Sun D, Zou Y, Liu Y, Huang L (2021) Two nanoformulations induce reactive oxygen species and immunogenetic cell death for synergistic chemo-immunotherapy eradicating colorectal cancer and hepatocellular carcinoma. Mol Cancer 20:10

Hamanishi J, Takeshima N, Katsumata N, Ushijima K, Kimura T, Takeuchi S, Matsumoto K, Ito K, Mandai M, Nakai H, Sakuragi N, Watari H, Takahashi N, Kato H, Hasegawa K, Yonemori K, Mizuno M, Takehara K, Niikura H, Sawasaki T, Nakao S, Saito T, Enomoto T, Nagase S, Suzuki N, Matsumoto T, Kondo E, Sonoda K, Aihara S, Aoki Y, Okamoto A, Takano H, Kobayashi H, Kato H, Terai Y, Takazawa A, Takahashi Y, Namba Y, Aoki D, Fujiwara K, Sugiyama T, Konishi I (2021) Nivolumab versus gemcitabine or pegylated liposomal doxorubicin for patients with platinum-resistant ovarian cancer: open-label, randomized trial in Japan (NINJA). J Clin Oncol 39:3671–3681

Hu WW, Syu WJ, Chen WY, Ruaan RC, Cheng YC, Chien CC, Li C, Chung CA, Tsao CW (2012) Use of biotinylated chitosan for substrate-mediated gene delivery. Bioconjug Chem 23:1587–1599

Hu H, Qi Q, Dong Z, Yu X, Mo Y, Luo J, Wang Y, Du S, Lu Y (2020) Albumin coated trimethyl chitosan-based targeting delivery platform for photothermal/chemo-synergistic cancer therapy. Carbohydr Polym 241:116335

Kuroki L, Guntupalli SR (2020) Treatment of epithelial ovarian cancer. BMJ 371:m3773

Lambert AW, Weinberg RA (2021) Linking EMT programmes to normal and neoplastic epithelial stem cells. Nat Rev Cancer 21:325–338
Lheureux S, Braunstein M, Oza AM (2019) Epithelial ovarian cancer: evolution of management in the era of precision medicine. CA A Cancer J Clin 69:280
Li Y, Zhang Y, Wang X, Yang Q, Zhou X, Wu J, Yang X, Zhao Y, Lin R, Xie Y, Yuan J, Zheng X, Wang S (2021) Bufalin induces mitochondrial dysfunction and promotes apoptosis of glioma cells by regulating annexin A2 and DRP1 protein expression. Cancer Cell Int 21:424
Liang L, Qiu L (2021) Vitamin E succinate with multiple functions: A versatile agent in nanomedicine-based cancer therapy and its delivery strategies. Int J Pharm 600:120457
Liang H, Yu T, Han Y, Jiang H, Wang C, You T, Zhao X, Shan H, Yang R, Yang L, Shan H, Gu Y (2018a) LncRNA PTAR promotes EMT and invasion-metastasis in serous ovarian cancer by competitively binding miR-101-3p to regulate ZEB1 expression. Mol Cancer 17:119
Liang H, Zhao X, Wang C, Sun J, Chen Y, Wang G, Fang L, Yang R, Yu M, Gu Y, Shan H (2018b) Systematic analyses reveal long non-coding RNA (PTAF)-mediated promotion of EMT and invasion-metastasis in serous ovarian cancer. Mol Cancer 17:96
Liao CC, Ho MY, Liang SM, Liang CM (2018) Autophagic degradation of SQSTM1 inhibits ovarian cancer motility by decreasing DICER1 and AGO2 to induce MIRLET7A-3P. Autophagy 14:2065–2082
Lu T, Tang J, Shrestha B, Heath BR, Hong L, Lei YL, Ljungman M, Neamati N (2020) Up-regulation of hypoxia-inducible factor antisense as a novel approach to treat ovarian cancer. Theranostics 10:6959–6976
Menon U, Gentry-Maharaj A, Burnell M, Singh N, Ryan A, Karpinskyj C, Carlino G, Taylor J, Massingham SK, Raikou M, Kalsi JK, Woolas R, Manchanda R, Arora R, Casey L, Dawnay A, Dobbs S, Leeson S, Mould T, Seif MW, Sharma A, Williamson K, Liu Y, Fallowfield L, McGuire AJ, Campbell S, Skates SJ, Jacobs IJ, Parmar M (2021) Ovarian cancer population screening and mortality after long-term follow-up in the UK collaborative trial of ovarian cancer screening (UKCTOCS): a randomised controlled trial. Lancet 397:2182–2193
Mitra R, Chen X, Greenawalt EJ, Maulik U, Jiang W, Zhao Z, Eischen CM (2017) Decoding critical long non-coding RNA in ovarian cancer epithelial-to-mesenchymal transition. Nat Commun 8:1604
Nieto MA, Huang RY, Jackson RA, Thiery JP (2016) Emt: 2016. Cell 166:21–45
Ning Z, Zhao Y, Yan X, Hua Y, Meng Z (2022) Flower-like composite material delivery of co-packaged lenvatinib and bufalin prevents the migration and invasion of cholangiocarcinoma. Nanomaterials 12:2048
Pan Z, Cai J, Lin J, Zhou H, Peng J, Liang J, Xia L, Yin Q, Zou B, Zheng J, Qiao L, Zhang L (2020) A novel protein encoded by circFNDC3B inhibits tumor progression and EMT through regulating Snail in colon cancer. Mol Cancer 19:71
Pandey NK, Xiong W, Wang L, Chen W, Bui B, Yang J, Amador E, Chen M, Xing C, Athavale AA, Hao Y, Feizi W, Lumata L (2022) Aggregation-induced emission luminogens for highly effective microwave dynamic therapy. Bioact Mater 7:112–125
Pastushenko I, Blanpain C (2019) EMT transition states during tumor progression and metastasis. Trends Cell Biol 29:212–226
Perry JL, Reuter KG, Luft JC, Pecot CV, Zamboni W, DeSimone JM (2017) "Mediating passive tumor accumulation through particle size tumor type, and location." Nano Lett 17:2879–2886
Pietila EA, Gonzalez-Molina J, Moyano-Galceran L, Jamalzadeh S, Zhang K, Lehtinen L, Turunen SP, Martins TA, Gultekin O, Lamminen T, Kaipio K, Joneborg U, Hynninen J, Hietanen S, Grenman S, Lehtonen R, Hautaniemi S, Carpen O, Carlson JW, Lehti K (2021) Co-evolution of matrisome and adaptive adhesion dynamics drives ovarian cancer chemoresistance. Nat Commun 12:3904
Pignata S, Lorusso D, Joly F, Gallo C, Colombo N, Sessa C, Bamias A, Salutari V, Selle F, Frezzini S, Giorgi UD, Pautier P, Bologna A, Orditura M, Dubot C, Gadducci A, Mammoliti S, Ray-Coquard I, Zafarana E, Breda E, Favier L, Ardizzoia A, Cinieri S, Largillier R, Sambataro D, Guardiola E, Lauria R, Pisano C, Raspagliesi F, Scambia G, Daniele G, Perrone F (2021) Carboplatin-based doublet plus bevacizumab beyond progression versus carboplatin-based doublet alone in patients with platinum-sensitive ovarian cancer: a randomised, phase 3 trial. Lancet Oncol 22:267–276
Pipaliya BV, Trofimova DN, Grange RL, Aeluri M, Deng X, Shah K, Craig AW, Allingham JS, Evans PA (2021) Truncated actin-targeting macrolide derivative blocks cancer cell motility and invasion of extracellular matrix. J Am Chem Soc 143:6847–6854
Poveda A, Floquet A, Ledermann JA, Asher R, Penson RT, Oza AM, Korach J, Huzarski T, Pignata S, Friedlander M, Baldoni A, Park-Simon T-W, Tamura K, Sonke GS, Lisyanskaya A, Kim J-H, Filho EA, Milenkova T, Lowe ES, Rowe P, Vergote I, Pujade-Lauraine E (2021) Olaparib tablets as maintenance therapy in patients with platinum-sensitive relapsed ovarian cancer and a BRCA1/2 mutation (SOLO2/ENGOT-Ov21): a final analysis of a double-blind, randomised, placebo-controlled, phase 3 trial. Lancet Oncol 22:620–631
Qian C, Wang J, Qian Y, Hu R, Zou J, Zhu C, Zhu Y, Qi S, Jia X, Wu L, Li W, Chen Z (2020) Tumor-cell-surface adherable peptide-drug conjugate prodrug nanoparticles inhibit tumor metastasis and augment treatment efficacy. Nano Lett 20:4153–4161
Rashidi LH, Homayoni H, Zou X, Liu L, Chen W (2016) Investigation of the strategies for targeting of the afterglow nanoparticles to tumor cells. Photodiagnosis Photodyn Ther 13:244–254
Shi Y, Lammers T (2019) Combining nanomedicine and immunotherapy. Acc Chem Res 52:1543–1554
Shi J, Kantoff PW, Wooster R, Farokhzad OC (2017) Cancer nanomedicine: progress, challenges and opportunities. Nat Rev Cancer 17:20–37
Shibue T, Weinberg RA (2017) EMT, CSCs, and drug resistance: the mechanistic link and clinical implications. Nat Rev Clin Oncol 14:611–629
Shrestha S, Wu J, Sah B, Vanasse A, Cooper LN, Ma L, Li G, Zheng H, Chen W, Antosh MP (2019) X-ray induced photodynamic therapy with copper-cysteamine nanoparticles in mice tumors. Proc Natl Acad Sci USA 116:16823–16828
Siegel RL, Miller KD, Fuchs HE, Jemal A (2021) Cancer statistics, 2021. CA Cancer J Clin 71:7–33
Su S, Dou H, Wang Z, Zhang Q (2021) Bufalin inhibits ovarian carcinoma via targeting mTOR/HIF-alpha pathway. Basic Clin Pharmacol Toxicol 128:224–233

Sung H, Ferlay J, Siegel RL, Laversanne M, Soerjomataram I, Jemal A, Bray F (2021) Global cancer statistics 2020: GLOBOCAN estimates of incidence and mortality worldwide for 36 cancers in 185 countries. CA Cancer J Clin 71:209–249
Tian X, Yin H, Zhang S, Luo Y, Xu K, Ma P, Sui C, Meng F, Liu Y, Jiang Y, Fang J (2014) Bufalin loaded biotinylated chitosan nanoparticles: an efficient drug delivery system for targeted chemotherapy against breast carcinoma. Eur J Pharm Biopharm 87:445–453
Torre LA, Trabert B, DeSantis CE, Miller KD, Samimi G, Runowicz CD, Gaudet MM, Jemal A, Siegel RL (2018) Ovarian cancer statistics, 2018. CA Cancer J Clin 68:284–296
Wang H, Zhang C, Xu L, Zang K, Ning Z, Jiang F, Chi H, Zhu X, Meng Z (2016) Bufalin suppresses hepatocellular carcinoma invasion and metastasis by targeting HIF-1alpha via the PI3K/AKT/mTOR pathway. Oncotarget 7:20193–20208
Wang R, Sun Q, Wang F, Liu Y, Li X, Chen T, Wu X, Tang H, Zhou M, Zhang S, Xiao Y, Huang W, Wang CC, Li L (2019) Efficacy and safety of Chinese herbal medicine on ovarian cancer after reduction surgery and adjuvant chemotherapy: a systematic review and meta-analysis. Front Oncol 9:730
Wen J, Yang K, Liu F, Li H, Xu Y, Sun S (2017) Diverse gatekeepers for mesoporous silica nanoparticle based drug delivery systems. Chem Soc Rev 46:6024–6045
Xu Y, Liu Y, Liu Q, Lu S, Chen X, Xu W, Shi F (2021) Co-delivery of bufalin and nintedanib via albumin sub-microspheres for synergistic cancer therapy. J Control Release 338:705–718
Yang H, Liu Y, Zhao MM, Guo Q, Zheng XK, Liu D, Zeng KW, Tu PF (2021a) Therapeutic potential of targeting membrane-spanning proteoglycan SDC4 in hepatocellular carcinoma. Cell Death Dis 12:492
Yang L, Zhou F, Zhuang Y, Liu Y, Xu L, Zhao H, Xiang Y, Dai X, Liu Z, Huang X, Wang L, Zhao C (2021b) Acetyl-bufalin shows potent efficacy against non-small-cell lung cancer by targeting the CDK9/STAT3 signalling pathway. Br J Cancer 124:645–657
Yuan Z, Yuan Y, Han L, Qiu Y, Huang X, Gao F, Fan G, Zhang Y, Tang X, He X, Xu K, Yin P (2018) Bufalin-loaded vitamin E succinate-grafted-chitosan oligosaccharide/RGD conjugated TPGS mixed micelles demonstrated improved antitumor activity against drug-resistant colon cancer. Int J Nanomed 13:7533–7548
Zeng H, Chen W, Zheng R, Zhang S, Ji JS, Zou X, Xia C, Sun K, Yang Z, Li H, Wang N, Han R, Liu S, Li H, Mu H, He Y, Xu Y, Fu Z, Zhou Y, Jiang J, Yang Y, Chen J, Wei K, Fan D, Wang J, Fu F, Zhao D, Song G, Chen J, Jiang C, Zhou X, Gu X, Jin F, Li Q, Li Y, Wu T, Yan C, Dong J, Hua Z, Baade P, Bray F, Jemal A, Yu XQ, He J (2018) Changing cancer survival in China during 2003–15: a pooled analysis of 17 population-based cancer registries. Lancet Glob Health 6:e555–e567
Zeng H, Xia C, Zhao B, Zhu M, Zhang H, Zhang D, Rui X, Li H, Yuan Y (2021) Folic acid-functionalized metal-organic framework nanoparticles as drug carriers improved bufalin antitumor activity against breast cancer. Front Pharmacol 12:747992
Zhang L, Nakaya K, Yoshida T, Kuroiwa Y (1992) Induction by bufalin of differentiation of human leukemia cells HL60, U937, and ML1 toward macrophage/monocyte-like cells and its potent synergistic effect on the differentiation of human leukemia cells in combination with other inducers. Cancer Res 52:4634–4641
Zhang JJ, Zhou XH, Zhou Y, Wang YG, Qian BZ, He AN, Shen Z, Hu HY, Yao Y (2019) Bufalin suppresses the migration and invasion of prostate cancer cells through HOTAIR, the sponge of miR-520b. Acta Pharmacol Sin 40:1228–1236
Zhou H, Liu Z, Zhang Z, Pandey NK, Amador E, Nguyen W, Chudal L, Xiong L, Chen W, Wen Y (2022) Copper-cysteamine nanoparticle-mediated microwave dynamic therapy improves cancer treatment with induction of ferroptosis. Bioact Mater 24:322–330
Zou D, Song J, Deng M, Ma Y, Yang C, Liu J, Wang S, Wen Z, Tang Y, Qu X, Zhang Y (2021) Bufalin inhibits peritoneal dissemination of gastric cancer through endothelial nitric oxide synthase-mitogen-activated protein kinases signaling pathway. FASEB J 35:e21601

Publisher's Note